Jurnal Tribologi 33 (2022) 97-112

MYTRIBOS Malaysian Tribology Society

Jurnal Tribologi

Website : jurnaltribologi.mytribos.org e-issn: 2289-7232

Deposit formation in the injector of a diesel engine fueled with higher blended palm biodiesel

Afiqah Hamzah [1,2], Ghazali Omar [1,2*], Mohd Zaid Akop [1,2], Mohd Hafidz Zakaria [1,3], Nur Natasha Atikah Rosli [1]

[1] Fakulti Kejuruteraan Mekanikal, Universiti Teknikal Malaysia Melaka, Hang Tuah Jaya, 76100 Durian Tunggal, Melaka, MALAYSIA.
[2] Centre of Advanced Research on Energy, Universiti Teknikal Malaysia Melaka, Hang Tuah Jaya, 76100 Durian Tunggal, Melaka, MALAYSIA.
[3] Jabatan Kejuruteraan Mekanikal, Politeknik Tuanku Syed Sirajuddin, MALAYSIA.
*Corresponding author: ghazali@utem.edu.my

KEYWORDS

Biodiesel-diesel blend
Internal injector deposit
Material compatibility

ABSTRACT

Diesel injection nozzles are precisely machined in the micrometre order to produce a fine fuel spray that is crucial for the engine's combustion and emission efficiency. This paper studies the deposition in a single-cylinder 4-stroke diesel engine fuel injector nozzle hole using higher blended biodiesel blends. Using B10 and B30, palm biodiesel blends in two separate engine runs, two sets of injectors are collected. The injectors are cross-sectioned to reveal the nozzle hole of the injectors. Scanning electron microscope (SEM), profilometer and electron dispersive X-ray spectroscopy (EDS) analysis of the injector hole surface are presented. The deposit structure is more precipitate type near the inlet and changes to multi-layered type near the outlet. The deposition in the fuel injector hole using a higher biodiesel percentage (B30) produce deposits with a bigger diameter as indicated by the 70% increase in average surface roughness than the deposition in the B10 injector hole.

Received 30 November 2021; received in revised form 9 February 2022; accepted 17 May 2022.
To cite this article: Hamzah et al. (2022). Deposit formation in the injector of a diesel engine fueled with higher blended palm biodiesel. Jurnal Tribologi 33, pp.97-112.

Nomenclature

ASTM	American Society for Testing and Materials
B10	10% by volume of palm biodiesel with fossil diesel
B30	30% by volume of palm biodiesel with fossil diesel
SEM	Scanning electron microscope
EDS	Electron dispersive X-ray spectroscopy
CO	Carbon monoxide
CO_2	Carbon dioxide
PM	Particulate matter
UHC	Unburned hydrocarbon
RPM	Revolutions per minute
SEI	Secondary electron
BSE	Back-scattered electron
R_a	arithmetical mean roughness
R_Y	Maximum height roughness
R_Z	Ten-point mean roughness

1.0 INTRODUCTION

The challenges to human society nowadays in tackling climate change is largely hindered by the insatiable consumption of natural resources to power human's daily life. The use of fossil fuel in many aspects from power generation, manufacturing and transportation is putting a toll on the environment from the production of greenhouse gases and other pollutants, causing global warming and health hazards (Abdullah et al., 2020). Recently, many communities around the globe are at risk of larger sized natural disasters such as floods and landslides when the delicate balance of the ecosystem is disturbed (Nicholls et al., 2021).

With the rising usage and imminent limited supply of fossil fuel, as well as mitigating the environmental impact of fossil fuel, the research society is geared towards finding more sustainable fuel sources. Biodiesel is regarded as the greatest contender for replacement mineral diesel in the transportation industry as it is easily adaptable to the existing vehicles (Dhar & Agarwal, 2014; Habibullah et al., 2015; Schemme et al., 2017). Transesterification of vegetable oils or animal fats permits fatty acid methyl or ethyl ester synthesis, typically termed biodiesel, which has similar physical qualities as mineral fuel (Kathpal, 2011).

The fundamental advantage of biodiesel is its compatibility with mineral fuel, allowing easy blending and substitution. Additionally, the inclusion of oxygen in the chemical structure of biodiesel allows complete combustion creating substantially lesser unburned hydrocarbon (UHC), carbon monoxide (CO), carbon dioxide (CO_2), sulfur dioxide (SO_2) and particulate matter (PM) emission (Abed et al., 2017; Sudrajat et al., 2020). It is also simply created from the mixing process and can be produced from several easily accessible feedstock (Mofijur et al., 2013; Unglert et al., 2020).

Despite these advantages, there are various problems with the usage of biodiesel in the engine. The biodiesel chemical composition includes corrosive and reactive components, which may cause faster depreciation of the engine components (Chandran et al., 2018; Fazal et al., 2014). The biodiesel physical qualities, such as viscosity and density, can affect the fuel injection process,

spray formation and droplet size (Slavinskas et al., 2018; Vinod Babu et al., 2017). Additionally, as biodiesel reacts with oxygen, it can create peroxide, organic acids and sticky sediments, causing sticking and deposition in the engine components (Komariah et al., 2018).

The fuel delivery system is a major vehicle system component since it determines its fuel efficiency and emissions. As technology improves to a more efficient system, injector nozzle holes diameter drops dramatically to generate better fuel spray. A common difficulty in a fuel injection system is internal injector deposit deposition. Careful design of the fuel injector ensures the proper creation of fuel spray, which is usually characterised by the spray length and droplets size, which is vital for complete combustion and cleaner emission. However, deposit accumulation in the fuel injector is likely to generate bigger fuel droplets, causing inefficient burning, increasing pollutant emissions, and diminishing fuel efficiency. In addition, injector internal deposit accumulation can cause failure in the injector charging mechanism, resulting in high maintenance costs and frequent replacement (Ueda et al., 2016). As more rigorous emission rules are adopted globally, there is an urgent need to research the formation of internal injector deposits (Hoang & Le, 2019a; Höök & Tang, 2013).

The study of deposition in the engine from using biodiesel have mostly dealt with deposition that occurs in the combustion chamber and on the surface of the fuel injector (Birgel et al., 2011; Liaquat et al., 2014; Reddy et al., 2018). The deposition that occurs inside the injector hole is significant as it could directly affect the fuel spray characteristics. The deposition mechanism in the injector hole differs from combustion chamber deposit as they are not directly exposed to combustion flame and heat, and is more dependent on the fuel physicochemical properties (Hoang et al., 2019). The small injector hole shape, usually about 100 μm magnitude, offered a challenge to investigate the interior hole deposition. Although various studies have successfully investigated internal hole deposition via x-ray spectroscopy, none has focused on deposition from the usage of palm biodiesel blends, which is necessary for the achievement of the Malaysian Biodiesel Mandate (McGilvery et al., 2020; Rounthwaite et al., 2017). Therefore, the current investigation evaluated the deposits created in the injector hole when using a higher proportion of palm biodiesel is blended in the fuel. Analysis of the deposit formation in the injector hole can provide valuable data on the possible spray characteristics and the overall engine performance when a higher palm biodiesel blend is used.

2.0 EXPERIMENTAL PROCEDURE

2.1 Materials

This study combined palm biodiesel with fossil diesel fuel at 10 and 30 % volume. Therefore, both samples are B10 and B30, respectively, depending on the blended palm biodiesel % volume. Samples are stored in a sealed container at ambient temperature, with as little exposure to light as feasible.

2.2 Method

The study covers four steps. In the first stage, the biodiesel-blend characteristics were measured using American Society for Testing and Materials (ASTM) standards. Then, an engine run experiment was undertaken for each fuel type. Next, injector samples are taken from the engine run experiment and cross-sectioned to examine the surface wear of the injector nozzle holes. Finally, a microscopic study was undertaken by measuring the injector hole surface

roughness using a profilometer, and spectroscopic analysis of the injector hole was conducted using Scanning Electron Microscope (SEM) and Energy Dispersive X-Ray Spectroscopy (EDS).

2.3 Properties Testing

The biodiesel-blend samples were examined for their primary physical properties: density, kinematic viscosity, flash point and water content. These were assessed using the ASTM standards stated in Table 1.

Table 1: ASTM standard referred for testing the physical properties of the biodiesel blends.

Properties (Unit)	ASTM
Density, ρ (g/mm^2)	ASTM D4052
Kinematic viscosity, (cP)	ASTM D751
Water content (ppm)	ASTM D2709
Flash point (°C)	ASTM D93

The density of the biodiesel blend was evaluated using a hydrometer. Measurements were taken three times, and the average value was calculated. First, measurement of the dynamic viscosity was done using a Brookfield Viscometer. Then, the kinematic viscosity was determined using the dynamic viscosity and density value. Next, a handheld infrared oil analyser, FluidScan 1000 Series, tested the fuel blend water content. Finally, the flashpoint was determined using the SETA Series 3 Closed Cup Flash Point Tester.

2.4 Engine Test Experiment

The engine test experiment comprises running a single-cylinder constant speed diesel engine utilising the two types of palm biodiesel blends, the B10 and B30. Sample injectors were sourced from a 1-hour engine test in a single-cylinder Esaco diesel engine model 178FA. The engine was warmed up before the test began. Throughout the test, the experiment was conducted at ambient temperature. A brand-new injector is fitted before testing each biodiesel blend. During the experiments, the fuel and the air temperature was at room temperature. The engine speed was always steady at roughly 2400 RPM. Further details of the test matrix are given in Table 2. Injectors are then imaged using a high magnification visualiser before being cross-sectioned utilising a wire electric discharge machining process.

Table 2: Test matrix for the experimental work.

Test No	Fuel Composition	Load Cycle	Fuel Temperature (^{o}C)	Air Temperature (^{o}C)
1	B10	Constant	30	30
2	B30	Constant	30	30

2.5 Injector Nozzle Cross-Sectioning

The injector nozzle hole has a very small diameter and requires a high precision cutting procedure. The placement of injector sectioning is depicted in Figure 1. In this work, the injectors were cross-sectioned using a submerged wire cutter. First, the placement of the nozzle hole is determined. Then, by subtracting the wire cutter diameter and nozzle hole radius from the magnitude of the injector radius, the wire cutter displacement can be obtained. The cross-sectioned injectors were then cleaned using a high-pressure air blower and placed in an ultrasonic

bath for 5 minutes before leaving to air dry for 1 to 2 hours. The cross-sectioned and cleaned injectors are then evaluated using spectroscopic analysis explained in the next section.

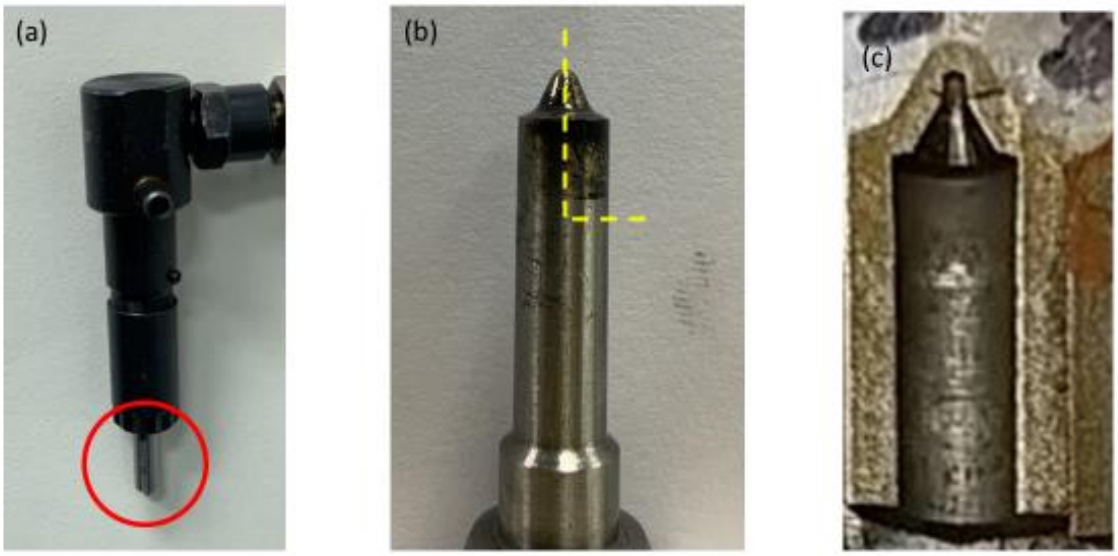

Figure 1: Process of cutting the injector to expose the injector hole (a) the injector tip is shown in the red circle (b) the cutting axis shown in yellow line is located at the hole to expose the nozzle hole (c) final cut injector showing nozzle hole at the injector tip.

2.6 Spectroscopic Analysis

Wear morphology and characterization investigation of the injector hole surface using scanning electron microscopy (SEM). Images studies were obtained using Jeol Scanning Electron Microscope coupled with energy dispersive x-ray spectrometer (EDS). In this methodology, secondary electrons (SEI) from material irradiated with a fine electron beam yield numerous signals that can be used to describe the surface topography. SEM can also be done using the backscattered electron (BSE) mode, detecting the compositional difference in the examined sample. BSE gives visual information based on grey-scale intensity between chemical phases. A specimen with a higher atomic number will generate a higher intensity of backscattered electrons. The generated image will have different brightness based on the specimen composition. In this investigation, both SEI and BSE images were employed to characterise the injector surface.

The elemental composition of a sample is determined using the characteristic X-ray spectra of the specimen being investigated. The elemental analysis was performed in a “spot mode” where the beam is localised on a specific location manually chosen within the range of view. By combining SEM with EDS, site-specific chemical analysis can be done for the region of interest. This approach permits the identification of most items and their position. The location is depicted on the given SEM pictures by a box. The EDS detector was capable of identifying elements with an atomic number equal to or greater than six. Therefore, the intensity of the peaks in the EDS is not a quantitative measure of elemental concentration, but relative amounts can be extrapolated from relative peak heights.

The injector samples were trimmed to 10mm in length and were joined to a multi-stub sample holder using double-sided conductive copper tape, following which it was mounted onto the specimen chamber. The specimen chamber and column were kept under vacuum. After reaching the vacuum target, the electron gun was activated and accelerating the voltage of 20 kV, probe current of 227 pA, and a working distance of 8.5 mm was preserved during the entire process.

2.7 Surface Roughness Measurement

Measurement of the injector hole surface roughness was done to determine the changes and severity of deposit formation. Measurement of surface roughness is typically done using a profilometer divided into two types: contact and non-contact profilometer. A contact profilometer uses a minuscule probe that touches the surface and detects the changes in surface height. However, this method has a setback as it can sometimes miss areas smaller than the probe diameter. A 3D non-contact profilometer uses laser and reflected light to measure the changes in surface heights and thus is more reliable. The measurement of surface roughness is presented in several forms, namely the arithmetical mean roughness (R_a), maximum height roughness (R_Y), and ten-point mean roughness (R_Z). R_a give the average surface roughness while R_Z measures the porosity of the surface. In this study, the 3D non-contact profilometer is used to measure the surface roughness of the injector hole at both the inlet and the outlet.

3.0 RESULTS AND DISCUSSION

3.1 Fuel Properties

Measurement of the biodiesel blends fuel properties used in this study is presented in Figure 2. Overall, the density, kinematic viscosity and flashpoint of the B10 is lower than B30. Higher biodiesel volume percentage in the blend contributed to higher fuel density. The higher density and kinematic viscosity are due to the higher degree of saturation and longer chain length in palm biodiesel compared to mineral diesel (Ali et al., 2017). In contrast, the B10 blend's water content is higher compared to the B30. Water content in biodiesel blend is expected to be lower in blends with a lower concentration of unsaturated bond (Jakeria et al., 2014). However, the presence of oxidation products might attract more moisture and cause higher water content. This suggests a higher oxidation product in the B10 blend compared to the B30 blend used in this study.

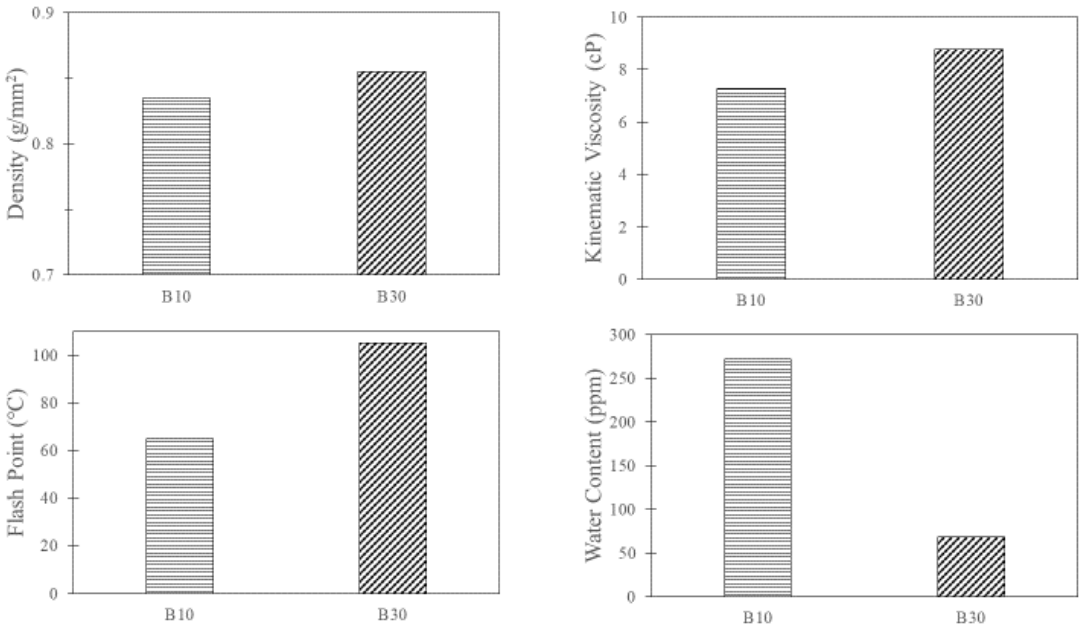

Figure 2: Comparison of the physical properties of B10 and B30 biodiesel blends.

3.2 Injector Visual Inspection

Visual inspection of the injectors was done to check on deposit build-up on the injectors. Figure 3 shows a close-up view of the injectors after a 1-hour engine run. The inspection presented no significant difference between the two injectors. However, there seems to be more soot accumulation on the injector for the B30 blend compared to the B10 blend.

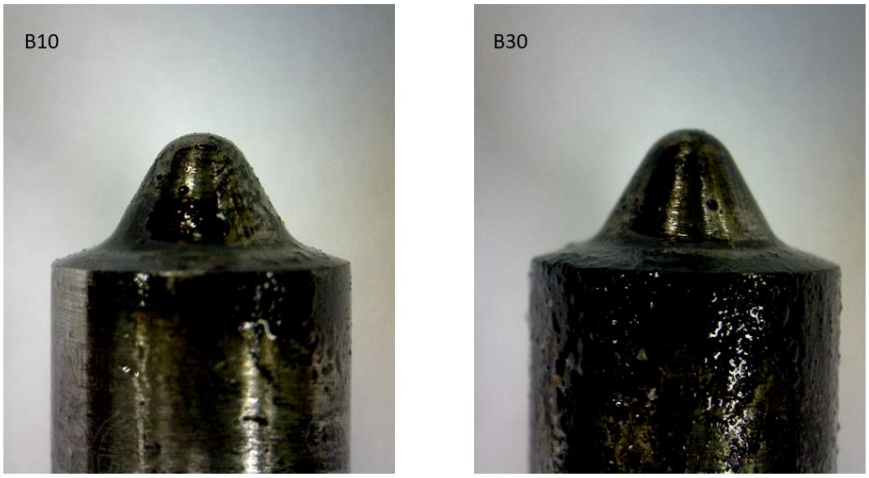

Figure 3: Close up view of the injectors before cross-sectioning. Injector used during B10 run on the left and B30 on the right.

3.3 Scanning Electron Microscopy (SEM)

Machining fuel injector nozzle demands great precision due to the requirement to generate several small diameter holes <300 μm with thick walls. Some injector holes are built with a tapered diameter to create a hydraulic environment that favours cavitation to produce finer spray droplets (Hao, 2013). The shape of the injector hole employed in this investigation measures around 200 μm, with no taper. Usually, machining of these tiny holes was done using laser, which forms stripes from recast layers on the injector hole wall (Blau et al., 2011).

Cross sectioning of the B10 injector has exposed the nozzle hole over its entire length. Figure 4 shows the cross-sectioned nozzle hole of the B10 injector on the left, with the image from SEI mode in the middle and BSE mode on the right. The tapered shape of the injector is due to small misalignment during the wire-cutting operation. Observation of the injector wall surface shows the wall is coated with precipitate or spherical type deposits with a diameter of roughly 1 μm. This deposition is consistent throughout the injector hole surface from the inlet to the outlet. At the B10 injector hole exit, a cluster of bigger diameter precipitates is discovered, with a diameter in the order of 10 μm. The BSE image of the injector wall surface at the inlet and outlet reveals a uniform brightness across the surface, with a slight shadow due to the injector hole curvature, indicating an overall uniform wall deposit composition throughout the injector hole.

Figure 5 shows the cross-section nozzle hole of the B30 injector. The precipitate deposition on the B30 injector hole surface appears to be two times greater in diameter than those in the B10 injector hole. The location of the depositions is localised at the machining burr lines on the injection hole wall surface. Larger sized depositions clusters are also found in both injector holes. However, in the B10 injector, these depositions are positioned near the hole outlet. While in the B30 injector hole, they are situated more towards the centre of the injector hole. The overall finding suggests higher biodiesel blend will give less deposition in the inner wall of the injector. However, the issue of the multi-layered deposition at the injector outlet should still be addressed.

Figure 6 gives the details of multi-layered deposition near the injector hole outlet of the B30 injector hole. The deposition near the outlet when using B30 seems to be more severe with multi-layer deposition is seen. A 1,500x magnification near the hole outlet shows a secondary deposition layer on top of the precipitate deposition. When seen using BSE mode, the secondary layer indicates it is made up of a different composition than the first layer of deposition. The higher temperature at the injector outlet and poor fuel atomization produces a multi-layered deposition structure from film type deposits produced from incomplete combustion product (Dearn et al., 2014). The temperature effect can also induce speciation of higher mass carbonaceous ions which can partly explain the differing deposit composition and type (Edney et al., 2020). The composition of the deposition layer is explained in detail in Section 3.4 by using EDS analysis.

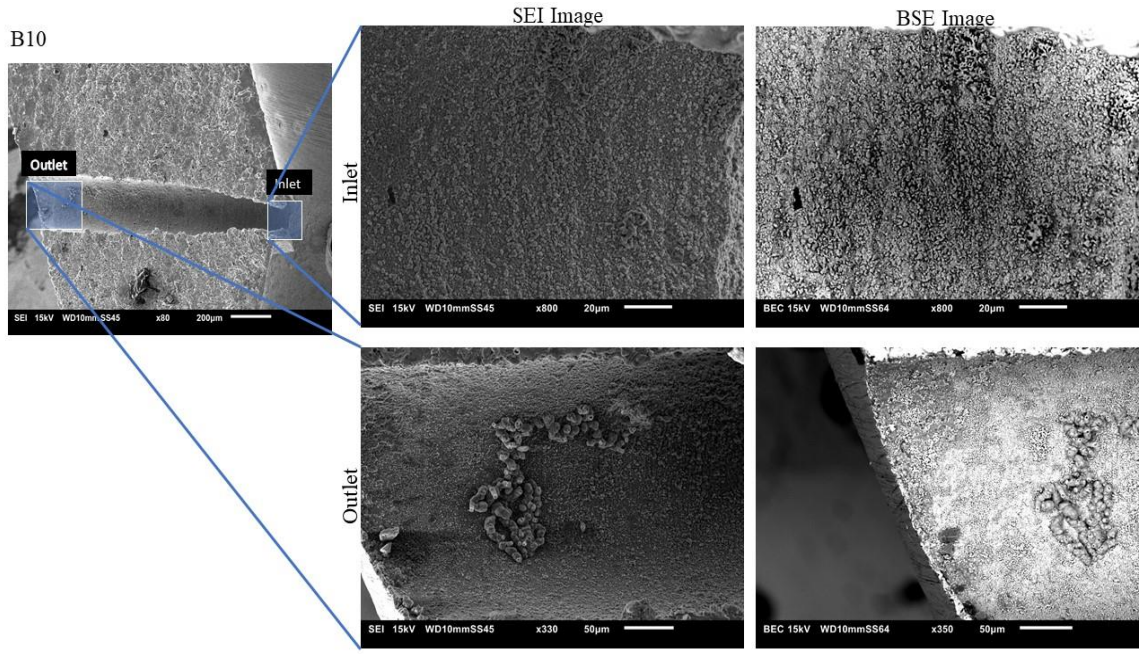

Figure 4: SEM image showing the surface characteristics of the B10 fuel injector hole internal wall.

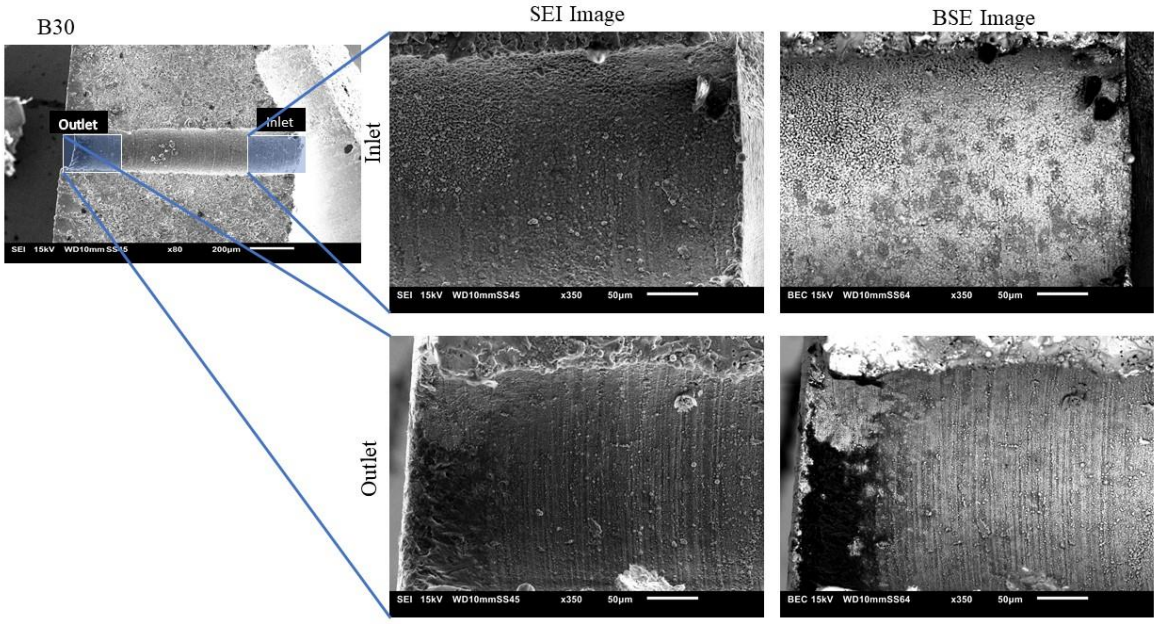

Figure 5: SEM image showing the surface characteristics of the B10 fuel injector hole internal wall.

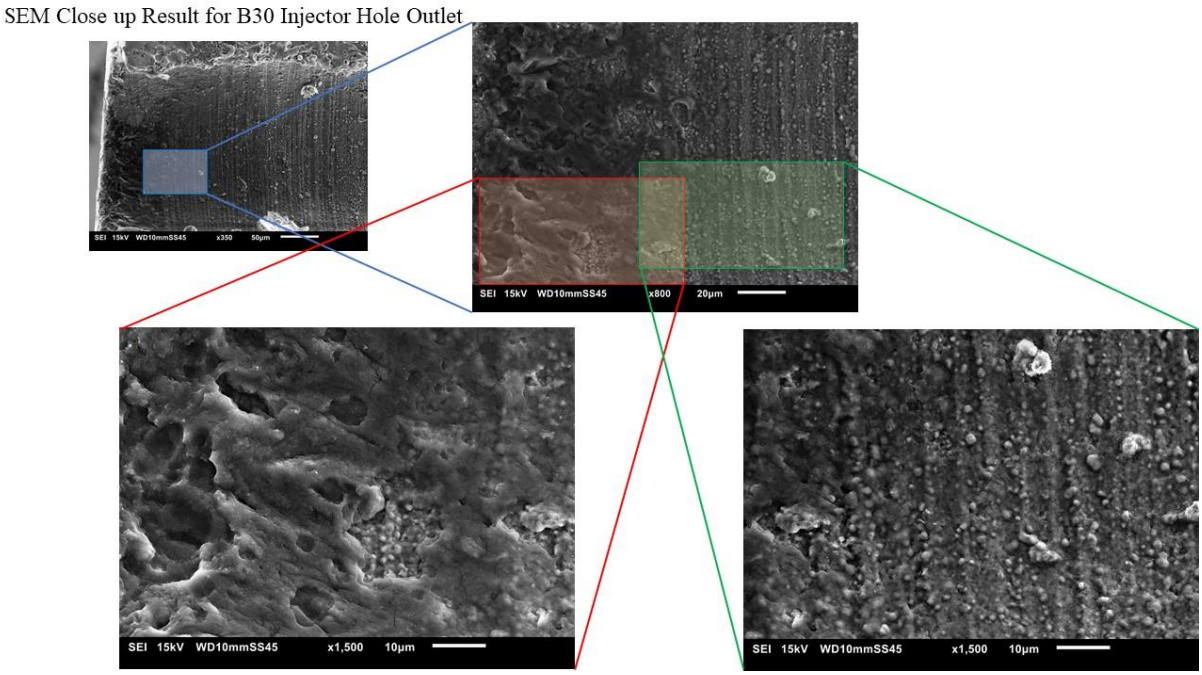

Figure 6: Multi-layer deposition near the outlet of the B30 injector hole.

Based on the observation of the SEM images, some correlation between fuel physicochemical properties and deposit formation mechanism in the fuel injector hole can be derived. In the B10 injector hole, the deposit forms mostly in precipitate type and is uniform from the inlet to the outlet of the injector hole. Similarly, for the B30 injector, a precipitate type deposit is seen along the injector hole wall, with a multi-layered type deposit near the outlet. Formation of the precipitate type deposit is suggested by Alves-Fortunato et al to be from oxidation products which are formed in the liquid phase of the fuel/ these precursor to deposit is not induced by the surface in contact with the fuel (Alves-Fortunato et al., 2020). The amount of auto-oxidation is more prevalent in biodiesel compared to fossil diesel, therefore it is observed B30 injector hole has to sustain bigger and thicker deposit formation compared to the B10 injector. This can be confirmed by the EDS and profilometer data in the next section. The second type of deposit structure, which is the multi-layered deposit structure is seen at the outlet of the B30 fuel injector hole is influenced by the higher kinematic viscosity and density of the B30 blends. The higher kinematic viscosity produces a less volatile mixture which can produce larger fuel droplets in the fuel spray, allowing more time for the deposit to form near the injector outlet (Hoang & Le, 2019b). In contrast, the B10 injector outlet does not show this type of deposition due to its lower kinematic viscosity.

3.4 Energy-Dispersive X-Ray Spectroscopy (EDS)

From SEM analysis in the previous sections, the general pattern of the deposit structure is similar between the two injectors, with the deposit structure changing from precipitate type to a multi-layered type from the inlet through to the outlet of the injector. This is in agreement with findings from other research (Rounthwaite et al., 2017). In this section, the chemical composition of the deposit on the injector hole surface is going to be analysed using EDS.

Figure 7 shows the material composition at the B10 inlet and outlet. At the inlet, the overall nozzle wall is covered with deposits. EDS analysis at the B19 injector inlet indicates the presence of Chromium, Iron, Manganese and Terbium. These compounds are materials that make up the alloy of diesel fuel injectors (Allocca et al., 2021; Molnar, 2007). Detection of these materials indicates the surface of the original injector wall is not fully covered by the carbon deposits. This composition is observed to be uniform from the inlet to the outlet.

However, some depositions are much larger in diameter near the outlet, as seen on the right of Figure 4. These bigger-sized depositions have covered the injector wall surface as indicated by EDS reading, which does not detect chromium and other metals that make up the injector material. The oxygen content of these larger sized depositions is double the ones detected at the inlet. Lastly, from Figure 8, the top layer of deposit at the B30 injector outlet shows a highly carbonaceous deposit (65.67%wt C). This layer is formed when there is incomplete combustion of the injected fuel, forming a film type deposit on top of the precipitate type deposit (Hoang et al., 2019; Yusmady, 2009)

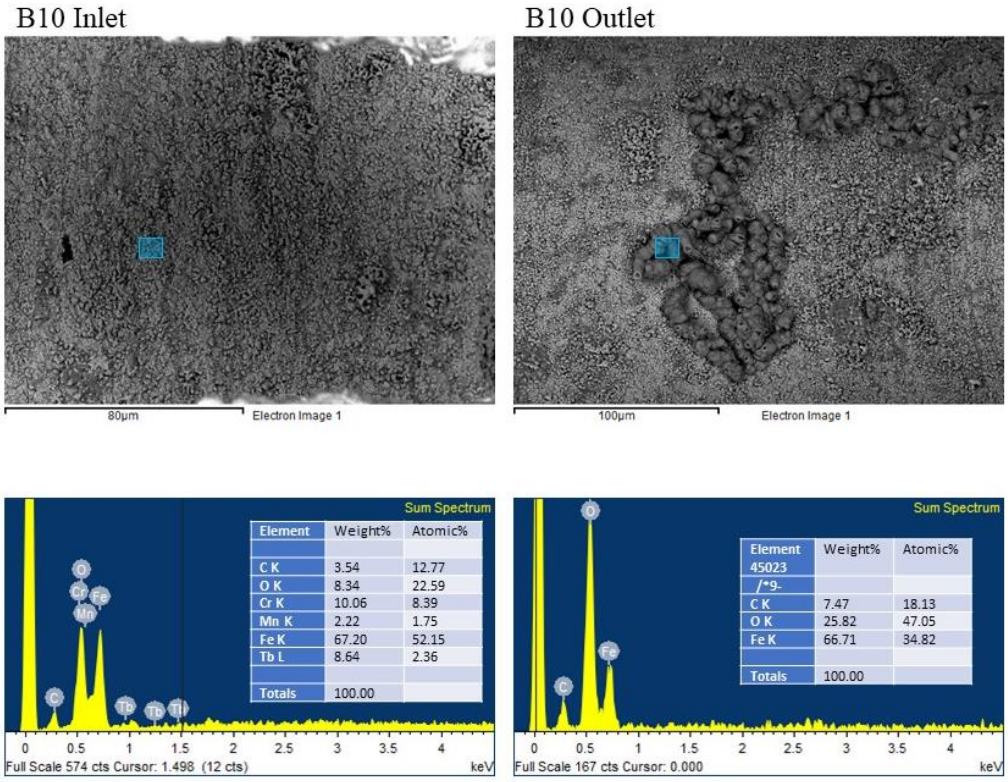

Figure 7: EDS analysis of the deposition composition of the B10 injector hole wall surface.

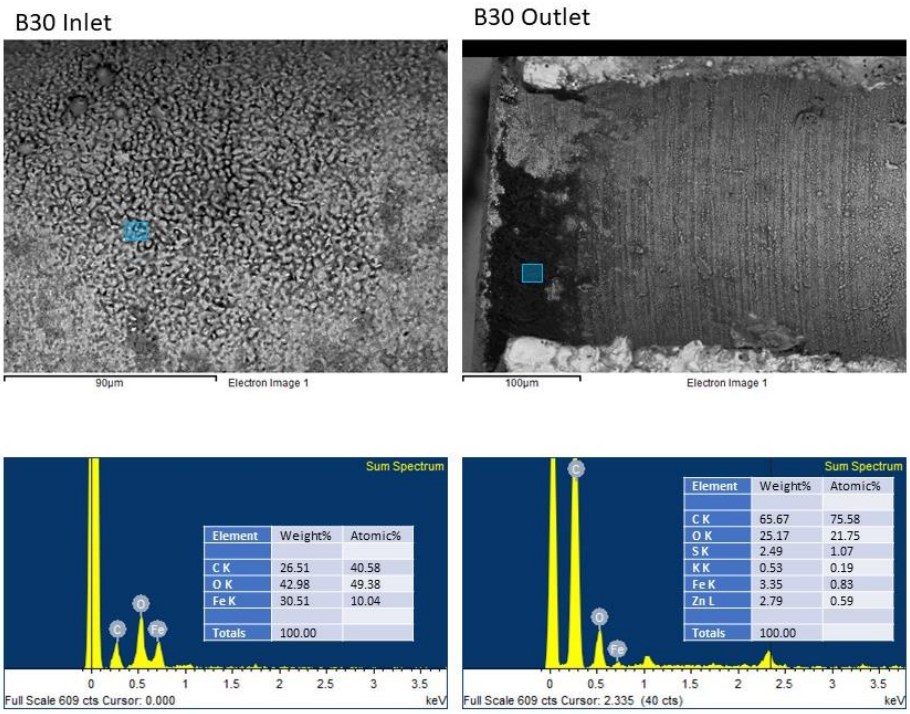

Figure 8: EDS analysis of the deposition composition of the B30 injector hole wall surface.

3.5 Profilometer

Table 3 shows the measurement of the injector hole wall roughness. The measurement is given in terms of average roughness (Ra) and the ten-point height (Rz), which measured the difference between the average of the highest five peaks and the lowest five valleys of a surface roughness profile. The R_a measurement of the B10 and B30 hole injector surface show the roughness in the B30 injector is 70% more rough compared to the B10 injector hole surface. Meanwhile, on average, the R_Z value for the B30 injector hole is 82% more compared to R_Z on the B10 injector hole. This means the surface in the B10 injector hole has more uniform surface roughness compared to the B30 injector hole. This is in agreement with the observation in the SEM images, which shows the deposition in the B10 injector hole has smaller diameters and is more uniform while the deposits in the B30 injector has bigger diameters.

Table 3 Surface roughness measurement of the nozzle hole at the inlet and outlet.

	Ra [µm]	**Rz [µm]**
B10 Inlet	1.07	5.23
B10 outlet	1.17	5.87
B30 Inlet	1.83	9.53
B30 outlet	1.97	10.90

The profilometer reading indicates the surface roughness of the fuel injector hole is increased when using the B30 blend. The increased surface roughness can affect the spray characteristics

from the turbulence-induced mechanism. A previous study on palm biodiesel fuel spray observed similar spray characteristics (spray angle and penetration length) with diesel fuel (Bohl et al., 2017). However, the spray characteristics are outside of the scope of this study and will be addressed in a future study.

CONCLUSION

Based on the experimental results, the influences of a higher percentage of palm biodiesel in the biodiesel-diesel blend (B30 vs B10) on deposit formation in the fuel injector hole were evaluated. The findings were summarized as follow:

(a) SEM analysis of the B10 and B30 injector surface wall shows a precipitate type deposit that can be formed from oxidation product in the fuel blend.
(b) A multi-layered deposition structure observed in the B30 fuel injector can be due to the B30 fuel higher kinematic viscosity and density, which produce bigger fuel droplets, allowing more deposits to be formed.
(c) EDS analysis indicates the deposits n B30 fuel injector hole is thicker as the original material of the fuel injector is not detected.
(d) This is confirmed from profilometer analysis, which shows the B30 injector hole has 70% increase in surface roughness and 82% increase in porosity.

As the current study only dealt with short term engine runs, future studies which include longer engine runs will be beneficial to see the deposition growth process in the fuel injector from prolonged use of higher biodiesel blend. The effect of turbulence and deposit washout on the overall injector hole deposition might not be accounted for when the test was run in a short time.

ACKNOWLEDGMENTS

Part of the work in this paper has initially been accepted and presented at the ICE-SEAM 2021. The authors would like to thank the Malaysian Mining Company (formerly Petronas Penapisan Melaka) and Sime Darby Biodiesel Sdn Bhd for supplying pure diesel and biodiesel, respectively, for the study. We are also grateful to Anton Paar Malaysia Sdn Bhd for access to fuel properties testing equipment. Additionally, the research has been financially funded by the Universiti Teknikal Malaysia Melaka under the Short Term Research Grant (PJP/2019/FKM(9A)/S01682).

REFERENCES

Abdullah, S., Abu, A., Nazmi, N., Mohd, L., Nurdiyana, W., & Mansor, W. (2020). Air quality status during 2020 Malaysia Movement Control Order (MCO) due to 2019 novel coronavirus (2019-nCoV) pandemic. Science of The Total Environment, 729(January), 139022. https://doi.org/10.1016/j.scitotenv.2020.139022

Abed, K. A., El-Diwani, G. I., El-Ibiari, N. N., El-Araby, R., El Morsi, A. K., & Gad, M. S. (2017). Performance and emissions characteristics of C.I. engine fueled with palm oil/palm oil methyl ester blended with diesel fuel. Egyptian Journal of Petroleum, 27(2), 215–219. https://doi.org/10.1016/j.ejpe.2017.05.009

Ali, O. M., Yusop, A. F., Rasul, M., Yasin, M. H. M., Mamat, R., Hamidi, M. A., & Ismail, M. Y. (2017). Study of Diesel-biodiesel Fuel Properties and Wavelet Analysis on Cyclic Variations in a Diesel Engine. Energy Procedia, 110(December 2016), 498–503.

https://doi.org/10.1016/j.egypro.2017.03.175
Allocca, L., Davino, D., Montanaro, A., & Visone, C. (2021). Proof of principle of a fuel injector based on a magnetostrictive actuator. Actuators, 10(9), 1–11. https://doi.org/10.3390/act10090237
Alves-Fortunato, M., Ayoub, E., Bacha, K., Mouret, A., & Dalmazzone, C. (2020). Fatty Acids Methyl Esters (FAME) autoxidation: New insights on insoluble deposit formation process in biofuels. Fuel, 268(April 2019), 117074. https://doi.org/10.1016/j.fuel.2020.117074
Birgel, A., Ladommatos, N., Aleiferis, P., Milovanović, N., Lacey, P., & Richards, P. (2011). Investigations on Deposit Formation in the Holes of Diesel Injector Nozzles. SAE International Journal of Fuels and Lubricants, 5, 123–131. https://doi.org/10.4271/2011-01-1924
Blau, P., Shyam, A., Hubbard, C., Howe, J., Trejo, R., Yang, N., & Pollard, M. (2011). Materials for high-pressure fuel injection systems.
Bohl, T., Tian, G., Smallbone, A., & Roskilly, A. P. (2017). Macroscopic spray characteristics of next-generation bio-derived diesel fuels in comparison to mineral diesel. Applied Energy, 186(2017), 562–573. https://doi.org/10.1016/j.apenergy.2016.10.082
Chandran, D., Gan, S., Lau, H. L. N., Raviadaran, R., Salim, M., & Khalid, M. (2018). Critical relationship between biodiesel fuel properties and degradation of fuel delivery materials of a diesel engine. Thermal Science and Engineering Progress, 7(November 2017), 20–26. https://doi.org/10.1016/j.tsep.2018.04.018
Dearn, K., Xu, J., Ding, H., Xu, H., Weall, A., Kirkby, P., Cooper, B., Edington, I., & Krueger-Venus, J. (2014). An Investigation into the Characteristics of DISI Injector Deposits Using Advanced Analytical Methods. SAE International Journal of Fuels and Lubricants, 7, 771–782. https://doi.org/10.4271/2014-01-2722
Dhar, A., & Agarwal, A. K. (2014). Effect of Karanja biodiesel blend on engine wear in a diesel engine. Fuel, 134, 81–89. https://doi.org/10.1016/j.fuel.2014.05.039
Edney, M. K., Lamb, J. S., Spanu, M., Smith, E. F., Steer, E., Wilmot, E., Reid, J., Barker, J., Alexander, M. R., Snape, C. E., & Scurr, D. J. (2020). Spatially Resolved Molecular Compositions of Insoluble Multilayer Deposits Responsible for Increased Pollution from Internal Combustion Engines. ACS Applied Materials and Interfaces, 12(45), 51026–51035. https://doi.org/10.1021/acsami.0c14532
Fazal, M. A., Haseeb, A. S. M. A., & Masjuki, H. H. (2014). A critical review on the tribological compatibility of automotive materials in palm biodiesel. Energy Conversion and Management, 79, 180–186. https://doi.org/10.1016/j.enconman.2013.12.002
Habibullah, M., Rizwanul Fattah, I. M., Masjuki, H. H., & Kalam, M. A. (2015). Effects of palm-coconut biodiesel blends on the performance and emission of a single-cylinder diesel engine. Energy and Fuels, 29(2), 734–743. https://doi.org/10.1021/ef502495n
Hoang, A. T., & Le, A. T. (2019a). A review on deposit formation in the injector of diesel engines running on biodiesel. Energy Sources, Part A: Recovery, Utilization and Environmental Effects, 41(5), 584–599. https://doi.org/10.1080/15567036.2018.1520342
Hoang, A. T., & Le, A. T. (2019b). Trilateral correlation of spray characteristics, combustion parameters, and deposit formation in the injector hole of a diesel engine running on preheated Jatropha oil and fossil diesel fuel. Biofuel Research Journal, 6(1), 909–919. https://doi.org/10.18331/BRJ2019.6.1.2
Hoang, A. T., Le, A. T., & Pham, V. V. (2019). A core correlation of spray characteristics, deposit formation, and combustion of a high-speed diesel engine fueled with Jatropha oil and diesel fuel. Fuel, 244(January), 159–175. https://doi.org/10.1016/j.fuel.2019.02.009

Höök, M., & Tang, X. (2013). Depletion of fossil fuels and anthropogenic climate change-A review. Energy Policy, 52, 797–809. https://doi.org/10.1016/j.enpol.2012.10.046

Jakeria, M. R., Fazal, M. A., & Haseeb, A. S. M. A. (2014). Influence of different factors on the stability of biodiesel: A review. Renewable and Sustainable Energy Reviews, 30, 154–163. https://doi.org/https://doi.org/10.1016/j.rser.2013.09.024

Kathpal, A. K. (2011). Utilization of Biodiesel for Rail Traction on Indian Railways. 1–10.

Komariah, L. N. N., Hadiah, F., Aprianjaya, F., & Nevriadi, F. (2018). Biodiesel effects on fuel filter; Assessment of clogging characteristics. Journal of Physics: Conference Series, 1095(1). https://doi.org/10.1088/1742-6596/1095/1/012017

Liaquat, A. M., Masjuki, H. H., Kalam, M. A., & Rizwanul Fattah, I. M. (2014). Impact of biodiesel blend on injector deposit formation. Energy, 72, 813–823. https://doi.org/10.1016/j.energy.2014.06.006

McGilvery, C. M., Jiang, J., Rounthwaite, N. J., Williams, R., Giuliani, F., & Britton, T. Ben. (2020). Characterisation of carbonaceous deposits on diesel injector nozzles. Fuel, 274(March), 117629. https://doi.org/10.1016/j.fuel.2020.117629

Mofijur, M., Masjuki, H. H. H., Kalam, M. A. A., Atabani, A. E. E., Shahabuddin, M., Palash, S. M. M., & Hazrat, M. A. A. (2013). Effect of biodiesel from various feedstocks on combustion characteristics engine durability and materials compatibility: A review. Renewable and Sustainable Energy Reviews, 28, 441–455. https://doi.org/10.1016/j.rser.2013.07.051

Molnar, J. R. (2007). Solenoid-type fuel injector assembly having stabilized ferritic stainless steel components (Patent No. US007252249B2).

Nicholls, R. J., Lincke, D., Hinkel, J., Brown, S., Vafeidis, A. T., Meyssignac, B., Hanson, S. E., Merkens, J. L., & Fang, J. (2021). Author Correction: A global analysis of subsidence, relative sea-level change and coastal flood exposure (Nature Climate Change, (2021), 11, 4, (338-342), 10.1038/s41558-021-00993-z). Nature Climate Change, 11(7), 634. https://doi.org/10.1038/s41558-021-01064-z

Reddy, S. M., Sharma, N., Gupta, N., & Agarwal, A. K. (2018). Effect of non-edible oil and its biodiesel on wear of fuel injection equipment components of a genset engine. Fuel, 222(March), 841–851. https://doi.org/10.1016/j.fuel.2018.02.132

Rounthwaite, N. J., Williams, R., Global, S., Uk, S., Mcgivery, C., Jiang, J., Giulliani, F., & Britton, B. (2017). A Chemical and Morphological Study of Diesel Injector Nozzle Deposits - Insights into their Formation and Growth Mechanisms. https://doi.org/10.4271/2017-01-0798

Schemme, S., Samsun, R. C., Peters, R., & Stolten, D. (2017). Power-to-fuel as a key to sustainable transport systems – An analysis of diesel fuels produced from CO2 and renewable electricity. Fuel, 205, 198–221. https://doi.org/https://doi.org/10.1016/j.fuel.2017.05.061

Slavinskas, S., Labeckas, G., & Mickevicius, T. (2018). Experimental study on injection characteristics of diesel and biodiesel fuel blends with common rail injection system. Engineering for Rural Development, 17, 2134–2140. https://doi.org/10.22616/ERDev2018.17.N504

Sudrajat, A., Tamaldin, N., Yamin, A. K. M., Abdollah, M. F. Bin, Zakaria, M. H., & Nyirenda, G. (2020). Performance analysis of biodiesel engine by addition of HHO gas as a secondary fuel. Jurnal Tribologi, 26(July), 120–134.

Ueda, D., Tanada, H., Utsunomiya, A., Kawamura, J., & Weber, J. (2016). 4th Generation Diesel Piezo Injector (Realizing Enhanced High Response Injector). SAE Technical Papers, 2016-April(April). https://doi.org/10.4271/2016-01-0846

Unglert, M., Bockey, D., Bofinger, C., Buchholz, B., Fisch, G., Luther, R., Müller, M., Schaper, K.,

Schmitt, J., Schröder, O., Schümann, U., Tschöke, H., Remmele, E., Wicht, R., Winkler, M., & Krahl, J. (2020). Action areas and the need for research in biofuels. Fuel, 268(January). https://doi.org/10.1016/j.fuel.2020.117227

Vinod Babu, V. B. M., Madhu Murthy, M. M. K., & Amba Prasad Rao, G. (2017). Butanol and pentanol: The promising biofuels for CI engines – A review. Renewable and Sustainable Energy Reviews, 78(April), 1068–1088. https://doi.org/10.1016/j.rser.2017.05.038

Yusmady, M. A. (2009). Diesel and Bio-diesel Fuel Deposits on a Hot Wall Surface (Issue August). Gunma University.